Added-Mass Effect in Modeling of Cilia-Based Devices for Microfluidic Systems

J. Kongthon

B. McKay

D. Iamratanakul

K. Oh

J.-H. Chung

J. Riley

S. Devasia[1]
e-mail: devasia@u.washington.edu

Department of Mechanical Engineering,
University of Washington,
Seattle, WA 98195-2600

This article shows that the added mass due to fluid-structure interaction significantly affects the vibrational dynamics of cilia-based (vibrating cantilever-type) devices for handling microscale fluid flows. Commonly, the hydrodynamic interaction between the cilia-based actuators and fluid is modeled as a drag force that results in damping of the cilia motion. Our main contribution is to show that such damping effects cannot explain the substantial reduction in the resonant-vibrational frequency of the cilia actuator operating in liquid when compared with the natural frequency of the cilia in air. It is shown that an added-mass approach (that accounts for the inertial loading of the fluid) can explain this reduction in the resonant-vibrational frequency when operating cantilever-type devices in liquids. Additionally, it is shown that the added-mass effect can explain why the cilia-vibration amplitude is not substantially reduced in a liquid by the hydrodynamic drag force. Thus, this article shows the need to model the added-mass effect, both theoretically and by using experimental results.
[DOI: 10.1115/1.4000766]

1 Introduction

This article reports on models for cilia-based devices (cantilever-type vibrating devices) for handling microscale fluid flows. Inspired by biological systems, cilia-based microactuators (that are excited by external vibrations or acoustic excitations) have been proposed for mixing and manipulating liquids in micro-/nanofluidic applications [1]. In such applications, models of the cilia dynamics are needed for optimizing the geometric design, as well as controlling the cilia to maximize the flow and minimize the required input energy. The challenge in modeling such cilia actuators is the coupling between the mechanical dynamics of the cilia and the fluid. Such coupling can lead to damping effects due to drag forces [2–4], which change the amplitude and resonant-vibrational frequency of the cilia when operated in liquid in contrast to operation in air or vacuum. However, the experimental results are presented in this article to show that the drag or damping effects are not sufficient to explain the substantial reduction in the resonant-vibrational frequency when the cilia actuators are operated in liquid (as opposed to the natural frequency when the cilia actuators are operated in air). The main contribution of this article is the use of an added-mass effect to account for this reduction in the natural frequency when cantilever-type devices are operated in a liquid. Thus, this article shows the need to include the added-mass effect (that accounts for the inertial loading of the liquid) when modeling the vibration of cantilever-type devices in a liquid medium.

Several works have modeled the vibrational dynamics of cilia-type (cantilever-type) devices operated in air [2,3], liquid [4,5], and vacuum [6–8]. The dynamics of these devices can be modeled as a second-order linear dynamic system, as shown in Ref. [2]. The drag force between the cilia actuators and the fluid affects the dynamics. The damping caused by the drag force can change the amplitude and resonant-vibrational frequency of the cilia actuators when operated in liquid in contrast to operation in air or vacuum. For example, the experimental results, presented in this article, show that the resonant-vibrational frequency $\omega_{r,w}=109.54$ Hz of the cilia actuators in water is substantially smaller than the natural frequency $\omega_{n,a}=338.68$ Hz of the cilia in air. However, this substantial reduction in the observed resonant-vibrational frequency is not predicted by standard second-order models for such cantilever structures, which yield a resonant-vibrational frequency expression of

$$\omega_{r,w} = \omega_{n,a}\sqrt{1-2\zeta^2} \tag{1}$$

where ζ is the damping ratio (e.g., see Ref. [9], Sec. 10.8). For example, the damping ratio ζ in a liquid tends to be in the range 0.05–0.5 [5]. For this range of the damping ratio, the anticipated resonant-vibrational frequency $\omega_{r,w}$ in a liquid is expected to be between $0.997\omega_{n,a}=337.66$ Hz and $0.707\omega_{n,a}=239.45$ Hz from Eq. (1). Note that this range (239.45–337.66 Hz) is much larger than the observed experimental value for the resonant-vibrational frequency in water of $\omega_{r,w}=109.54$ Hz. Thus, the damping effects are not sufficient to capture the change in the resonant-vibrational frequency of the cilia actuators when operated in liquids.

The main contribution of this article is to show that an added-mass effect is needed to account for the substantial reduction in the resonant-vibrational frequency of cantilever-type devices in liquids. It is noted that the added-mass effect is important in models of underwater vehicles, such as submarines [10], and was modeled in early works on pendulum oscillations initiated by Dubuat; the history of the added mass is provided by Stokes in Ref. [11]. Such an added-mass model is proposed to account for the substantial decrease in the vibrational natural frequency for cilia-type devices. The proposed added-mass model affects the natural frequency $\omega_{n,w}$ of the system in liquid, which in turn changes the resonant-vibrational frequency $\omega_{r,w}$. Such changes in the natural frequency $\omega_{n,w}$ are shown to occur in experimentally obtained models. Additionally, it is shown that the added-mass effect can explain why the cilia-vibration amplitude is not substantially reduced in a liquid by the hydrodynamic drag force. Thus, this article shows the need to capture the added-mass effect to model the vibration of cantilever-type devices in liquid media.

2 Dynamics of Cilium in Fluid

2.1 System Description. The displacement along the length (x) of a cilium is excited by the motion ($u(t)$) of the cilia base by using a piezostage (Burleigh PZS200), as shown in Fig. 1. The cilia are fabricated from polydimethylsiloxane (PDMS) using a silicon mold. Detailed information on cilia fabrication and material properties can be found in Ref. [1]. The nominal dimensions of the silicon mold used to fabricate the cilia used in the experiments are length ($L=800$ μm), height ($H=45$ μm), and depth ($D=10$ μm). The input to the system is the motion

[1]Corresponding author.

Contributed by the Technical Committee on Vibration and Sound of ASME for publication in the JOURNAL OF VIBRATION AND ACOUSTICS. Manuscript received January 31, 2008; final manuscript received November 25, 2009; published online February 12, 2010. Assoc. Editor: Bogdan I. Epureanu.

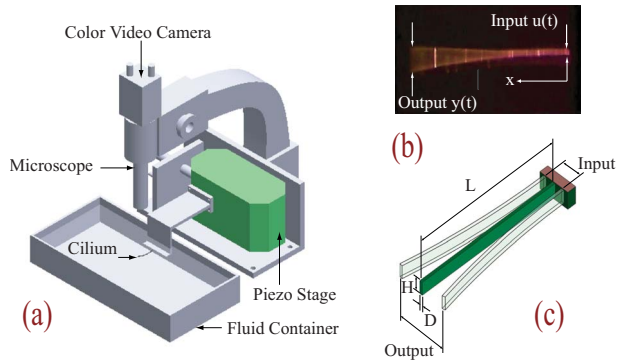

Fig. 1 (*a*) Experimental setup for testing the resonant-vibrational frequency of cilia. (*b*) Image of a cilium excited by piezostage. (*c*) Nominal cilium dimensions are length $L=800$ μm, depth $D=10$ μm, and height $H=45$ μm.

$$u(t) = A\ \sin(\omega t)$$

of the base of the cilia (actuated by the piezostage) and the output of the system is the motion

$$y(t) = \hat{y}(L,t)$$

of the cilia tip, i.e., at the free end with $x=L$, as shown in Fig. 1. The input (cilia-base motion $u(t)$) and the output (cilia-tip motion $y(t)$) are observed by using an optical microscope (Bausch & Lomb MicroZoom II High Performance Microscope with an attached Sony Color Video Camera 3CCD) and the displacement of the vibrating cilia is measured using captured still images (PINNACLE STUDIO Version 9.4.3). Two cases are studied: (a) cilia vibrating in air and (b) cilia vibrating when immersed in water—the fluid container (see Fig. 1) is stationary. An example image of cilia vibrating in fluid is shown in Fig. 1.

2.2 Experimental Frequency Response. The experimentally measured, input-to-output responses of the cilia (of nominal length $L=800$ μm) are shown in Fig. 2 for two cases: (case a) cilia in air and (case b) cilia in de-ionized (DI) water. The input-to-output frequency responses in Fig. 2 show a sharp increase in the output to input ratio near the resonant-vibrational frequencies. Note that the resonant-vibrational frequency $\omega_{r,w}=109.54$ Hz of the cilia actuators in water is substantially smaller than the resonant-vibrational frequency $\omega_{r,a}=336.05$ Hz of the cilia in air.

Table 1 Experimental fit of the parameters in Eq. (2) for six cilia actuated in air ($L=800$ μm), where σ represents the standard deviation and $K=1.566$

	ζ_1	ζ_2	$\omega_{n,a}$ (Hz)	$\omega_{r,a}$ (Hz)
Cilium 1	0.143	0.166	340.2	337.56
Cilium 2	0.145	0.167	340.8	338.12
Cilium 3	0.142	0.165	336.4	333.82
Cilium 4	0.145	0.167	336.9	334.25
Cilium 5	0.144	0.166	341.1	338.45
Cilium 6	0.145	0.166	336.7	334.09
Mean	0.1440	0.1662	338.68	336.05
σ	0.0013	0.0008	2.23	2.21

2.3 Model of the Frequency Response. The experimental frequency responses (in air and in water) can be captured using simplified, second-order, linear models of the following form (similar to Refs. [2,12])

$$G(s) = \frac{Y(s)}{U(s)} = \frac{-K(s^2 + 2\zeta_1\omega_n s)}{s^2 + 2\zeta_2\omega_n s + \omega_n^2} + 1 \tag{2}$$

where $G(s)$ is the transfer function in the Laplace domain, K is a constant related to the transfer function's gain, ω_n is the natural frequency, and ζ_1, ζ_2 are the damping ratios. It is noted that at small input frequencies (i.e., when $s \to 0$), the transfer function in Eq. (2) approaches 1 ($G(s) \to 1$), which implies that the tip displacement is similar to the base displacement. The parameters of the model, found by minimizing the least-squares-error between the predicted and measured frequency responses, are presented in Tables 1 and 2. The fitted model captures the experimental frequency response, as shown in Fig. 2.

2.4 Reduction in Natural Frequency. There is a substantial reduction in the resonant-vibrational frequency and the natural frequency when the cilia are actuated in water in comparison to the case when the cilia are actuated in air, as seen in Tables 1 and 2. For example, the resonant-vibrational frequency drops from 336.05 Hz to 109.54 Hz and the natural frequency drops from 338.68. Hz to 116.70 Hz. The considerable decrease in the natural frequency (and the associated resonance frequency) cannot be explained by a standard model that predicts the natural frequency ω_n for a cantilever beam to be [13]

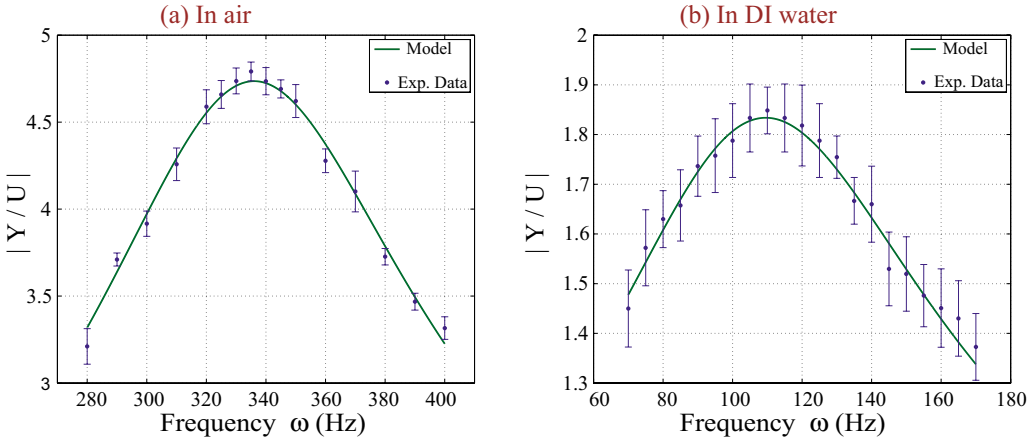

Fig. 2 Frequency response of cilia with nominal dimensions $L\times H\times D=800\times 45\times 10$ μm^3 in (*a*) air and (*b*) DI water. The dots represent the experimental data (mean value of six cilia), and the bars represent the standard deviation $\pm\sigma$. The lines represent the response of the model in Eq. (2) with the fitted parameters in Tables 1 and 2.

Table 2 Experimental fit of the parameters in Eq. (2) for cilia actuated in DI water ($L=800$ μm), where σ represents the standard deviation and $K=1.566$

	ζ_1	ζ_2	$\omega_{n,w}$ (Hz)	$\omega_{r,w}$ (Hz)
Cilium 1	0.43	0.45	116.4	109.19
Cilium 2	0.45	0.46	114.5	107.15
Cilium 3	0.44	0.45	117.6	110.40
Cilium 4	0.43	0.44	118.2	111.31
Cilium 5	0.44	0.45	114.1	107.12
Cilium 6	0.44	0.45	119.4	112.09
Mean	0.438	0.450	116.70	109.54
σ	0.008	0.006	2.10	2.10

$$\omega_n = \omega_{n,a} = \omega_{n,w} = \left(\frac{1.875^2}{L^2}\right)\sqrt{\frac{EI}{\rho_b A_b}} = \beta^2\sqrt{\frac{EI}{\rho_b A_b}} \tag{3}$$

where ρ_b is the mass density, $A_b=DH$ is the cross-sectional area, $I=HD^3/12$ is the area moment of inertia, and E is Young's modulus. Note that the natural frequency expression (in Eq. (3)) does not depend on the fluid properties nor on damping effects. Therefore, there is a need to reformulate the model to include fluid effects to capture the reduction in natural frequency when operating in fluids, in particular, to include the effect of inertial loading of the fluid on the cantilever. The modeling of this added-mass effect is discussed in Sec. 3.

3 Theoretical Modeling

To predict the experimental second-order response in Eq. (2), a model can be developed by using the Euler–Bernoulli beam approach [2,3,13], as shown next.

3.1 Standard Beam Model Without Added-Mass Effect. The standard Euler–Bernoulli beam approach [12,13] to describe the net motion $\hat{y}(x,t)$ of a vibrating cilium (beam) is

$$\rho_b A_b\frac{\partial^2\hat{y}(x,t)}{\partial t^2} + EI\frac{\partial^4\hat{y}(x,t)}{\partial x^4} = f(x,t) \tag{4}$$

where the subscript b represents a property of the beam, the subscript w represents a property of the water (liquid), and the net motion $\hat{y}(x,t)$ is composed of the base motion, i.e., the input $u(t)=A\sin(\omega t)$ and the elastic deflection, $\hat{w}(x,t)$ of the cilium (beam):

$$\hat{y}(x,t) = \hat{w}(x,t) + u(t) \tag{5}$$

The first term on the left hand side of Eq. (4) represents the inertial effects, the second term on the left hand side of Eq. (4) represents the elastic effects, and $f(x,t)$ represents the external forces (per unit length), which is composed of two damping terms:

$$f(x,t) = f_f(x,t) + f_i(x,t) \tag{6}$$

In the above equation, f_f is the distributed drag force due to hydrodynamic interaction that depends on the relative velocity between the structure and the fluid; it is approximated as (similar to Refs. [2,3])

$$f_f(x,t) = -B_f\left[\frac{\partial\hat{y}(x,t)}{\partial t} - V_f\right] = -B_f\left[\frac{\partial\hat{y}(x,t)}{\partial t}\right] \tag{7}$$

where B_f is the fluid damping parameter that depends on the flow conditions, and V_f is the fluid velocity, which is zero in the current experimental setup. The internal damping force f_i per unit length (in Eq. (6)) that depends on the rate of change of the beam's elastic deflection is

$$f_i(x,t) = -B_i\left(\frac{\partial\hat{w}(x,t)}{\partial t}\right) \tag{8}$$

where B_i is the internal damping parameter that depends on the beam properties. Applying the distributed fluid drag force, f_f, in Eq. (7) and the distributed internal damping force, f_i, in Eq. (8) as external forces, the Euler–Bernoulli equation (Eq. (4)) becomes, in the terms of the beam deflection $\hat{w}$ and base motion u (in Eq. (5)),

$$\rho_b A_b\frac{\partial^2\hat{w}(x,t)}{\partial t^2} + (B_f+B_i)\frac{\partial\hat{w}(x,t)}{\partial t} + EI\frac{\partial^4\hat{w}(x,t)}{\partial x^4} = -B_f\dot{u}(t) - \rho_b A_b\ddot{u}(t) \tag{9}$$

with the standard cantilever boundary conditions:

$$\hat{w}(0,t)=0, \quad \frac{\partial\hat{w}(0,t)}{\partial x}=0, \quad \frac{\partial^2\hat{w}(L,t)}{\partial x^2}=0, \quad \frac{\partial^3\hat{w}(L,t)}{\partial x^3}=0 \tag{10}$$

3.2 Modeling the Added-Mass Effect. The added-mass effect arises because of the need to accelerate the fluid around an object when it is accelerated through a fluid [11,14–16]. The inertia of the fluid exerts a resistive force on the body; this resistive force is termed as the *added-mass effect* because the body responds as if its mass has increased. This added-mass of the body depends on the medium in which the body (cilia actuator) is moving. This added-mass effect can be modeled with an additional inertial forcing term (f_m) to the external force f in Eq. (6), which becomes

$$f(x,t) = f_f(x,t) + f_i(x,t) + f_m(x,t) \tag{11}$$

with

$$f_m(x,t) = -\rho_w A_w\frac{\partial^2\hat{y}(x,t)}{\partial t^2} = -C_m\rho_b A_b\frac{\partial^2\hat{y}(x,t)}{\partial t^2} = -C_m\rho_b A_b\left(\frac{\partial^2\hat{w}(x,t)}{\partial t^2} + \ddot{u}(t)\right) \tag{12}$$

where A_w is the effective hydrodynamic area of the fluid that affects the inertial force f_m (per unit length), ρ_b is the beam density, and

$$C_m = \frac{\rho_w A_w}{\rho_b A_b} \tag{13}$$

is the added-mass coefficient, which is zero if the added mass is zero. The beam equation (9), after dividing all terms with $\rho_b A_b(1+C_m)$, becomes

$$\frac{\partial^2\hat{w}(x,t)}{\partial t^2} + \frac{(B_f+B_i)}{\rho_b A_b(1+C_m)}\frac{\partial\hat{w}(x,t)}{\partial t} + \frac{EI}{\rho_b A_b(1+C_m)}\frac{\partial^4\hat{w}(x,t)}{\partial x^4} = r(t) \tag{14}$$

with the forcing term $r(t)$ given by

$$r(t) = -\ddot{u}(t) - \frac{B_f}{\rho_b A_b(1+C_m)}\dot{u}(t) \tag{15}$$

3.3 Transfer Function for First Vibrational Mode. The partial differential equation (14) is solved by substituting the following separation of variables:

$$\hat{w}(x,t) = \sum_{n=1}^{\infty} X_n(x)T_n(t) \tag{16}$$

for $\hat{w}$ into Eq. (14) to obtain

$$\sum_{n=1}^{\infty} X_n(x)\ddot{T}_n(t) + \frac{(B_f + B_i)}{\rho_b A_b(1 + C_m)} \sum_{n=1}^{\infty} X_n(x)\dot{T}_n(t) + \frac{EI}{\rho_b A_b(1 + C_m)} \sum_{n=1}^{\infty} X_n''''(x) T_n(t) = r(t). \tag{17}$$

Note that $X_n(x)$ represents the shape of the nth vibrational mode, which is obtained by considering the homogeneous equation with $r(t)=0$ in Eq. (17). The homogeneous equation is satisfied if each mode satisfies

$$X_n(x)\ddot{T}_n(t) + \frac{(B_f + B_i)}{\rho_b A_b(1 + C_m)} X_n(x)\dot{T}_n(t) + \frac{EI}{\rho_b A_b(1 + C_m)} X_n''''(x) T_n(t) = 0 \tag{18}$$

which can be rewritten as a function of x on one hand and a function of t on the other hand that are both constant $(-z^2)$, i.e.,

$$\frac{\ddot{T}_n(t)}{T_n(t)} + \frac{(B_f + B_i)}{\rho_b A_b(1 + C_m)} \frac{\dot{T}_n(t)}{T_n(t)} = -\frac{EI}{\rho_b A_b(1 + C_m)} \frac{X_n''''(x)}{X_n(x)} = -z^2.$$

This yields two equations

$$\ddot{T}_n(t) + \frac{(B_f + B_i)}{\rho_b A_b(1 + C_m)} \dot{T}_n(t) + z^2 T_n(t) = 0 \tag{19}$$

$$X_n''''(x) - \frac{\rho_b A_b(1 + C_m)}{EI} z^2 X_n(x) = 0 \tag{20}$$

Each mode shape X_n can be obtained from Eq. (20) as [13]

$$X_n(x) = \cosh(\beta_n x) - \cos(\beta_n x) - \sigma_n(\sinh(\beta_n x) - \sin(\beta_n x)) \tag{21}$$

where

$$X_n''''(x) = \beta_n^4 X_n(x) \tag{22}$$

$$\beta_n = \left[\frac{\rho_b A_b(1 + C_m)}{EI} z^2 \right]^{1/4} \tag{23}$$

For the first mode of vibration $X_1(x)$,

$$\beta_1 L = 1.875, \quad \sigma_1 = 0.7341 \tag{24}$$

Multiplying the nonhomogeneous equation (17) with the first mode $X_1(x)dx$ and integrating with respect to the length after using the mode shape property in Eq. (22) result in

$$\sum_{n=1}^{\infty} \int_0^L X_1(x)X_n(x)dx\ddot{T}_n(t) + \frac{(B_f + B_i)}{\rho_b A_b(1 + C_m)} \sum_{n=1}^{\infty} \int_0^L X_1(x)X_n(x)dx\dot{T}_n(t) + \frac{EI}{\rho_b A_b(1 + C_m)} \sum_{n=1}^{\infty} \int_0^L \beta_n^4 X_1(x)X_n(x)dx T_n(t) = r(t) \int_0^L X_1(x)dx$$

The orthogonality of the mode shapes results in only the first mode remaining after the integration in the above equation to yield

$$\ddot{T}_1(t) + \frac{(B_f + B_i)}{\rho_b A_b(1 + C_m)} \dot{T}_1(t) + \frac{EI}{\rho_b A_b(1 + C_m)} \beta_1^4 T_1(t) = r(t)K_1 \tag{25}$$

$$K_1 = \frac{\int_0^L X_1(x)dx}{\int_0^L X_1(x)X_1(x)dx} = \frac{0.783L}{L} = 0.783 \tag{26}$$

which can be rewritten (using r from Eq. (15)) as

$$\ddot{T}_1(t) + 2(\zeta_f + \zeta_i)\omega_n \dot{T}_1(t) + \omega_n^2 T_1(t) = -K_1[\ddot{u}(t) + 2\zeta_f \omega_n \dot{u}(t)] \tag{27}$$

where the natural frequency ω_n, the fluid damping ratio ζ_f, and the internal damping ratio ζ_i are given by

$$\omega_n = \left(\beta_1^2 \sqrt{\frac{EI}{\rho_b A_b}} \right) \frac{1}{\sqrt{(1 + C_m)}} = \frac{\omega_n^*}{\sqrt{(1 + C_m)}} \tag{28}$$

$$\zeta_f = \frac{1}{2\omega_n} \left(\frac{B_f}{\rho_b A_b(1 + C_m)} \right) = \frac{B_f}{2\beta_1^2 \sqrt{EI\rho_b A_b}} \frac{1}{\sqrt{(1 + C_m)}} = \frac{\zeta_f^*}{\sqrt{(1 + C_m)}} \tag{29}$$

$$\zeta_i = \frac{1}{2\omega_n} \left(\frac{B_i}{\rho_b A_b(1 + C_m)} \right) = \frac{B_i}{2\beta_1^2 \sqrt{EI\rho_b A_b}} \frac{1}{\sqrt{(1 + C_m)}} = \frac{\zeta_i^*}{\sqrt{(1 + C_m)}} \tag{30}$$

where ω_n^*, ζ_f^*, and ζ_i^* are the natural frequency, the fluid damping ratio, and the internal damping ratio, respectively, without the added-mass effect. The total tip displacement, due to the first vibrational mode X_1 and the base motion $u(t)$, is

$$y(t) = X_1(L)T_1(t) + u(t) = 2T_1(t) + u(t) \tag{31}$$

since (from Eq. (21)) $X_1(L)=2$. Taking the Laplace transform on both sides of Eq. (27) to find $T(s)$, substituting this expression for $T(s)$ into Eq. (31) (after taking the Laplace transform on both sides of Eq. (31)), and dividing Eq. (31) by $U(s)$ yield

$$G(s) = \frac{Y(s)}{U(s)} = \frac{-2K_1(s^2 + 2\zeta_f \omega_n s)}{s^2 + 2(\zeta_f + \zeta_i)\omega_n s + \omega_n^2} + 1 \tag{32}$$

which is the same as the experimental model (in Eq. (2)) with

$$K = 2K_1 = 1.566, \quad \zeta_1 = \zeta_f, \quad \zeta_2 = \zeta_f + \zeta_i \tag{33}$$

where the value of K_1 is from Eq. (26).

4 Discussion of Added-Mass Effect

This section begins with a discussion of the effective fluid area that influences the inertial loading to quantify the added-mass effect. This is followed by a comparative evaluation of models with and without the added-mass effect. In particular, it is shown that the added-mass effect (when compared with the case without the added mass) (i) lowers the resonant-vibrational frequency and (ii) increases the vibrational amplitude at resonance in liquid.

4.1 Quantifying the Added-Mass Effect. The added-mass coefficient C_m (in Eq. (13)) quantifies the added mass $\rho_w A_w$ (per unit length of the beam) in terms of the displaced mass $\rho_b A_b$. The value of the added-mass coefficient C_m, in water, is obtained by using Eq. (28) and Tables 1 and 2 as

$$C_m = \left(\frac{\omega_n^{*2}}{\omega_{n,w}^2} - 1 \right) \approx \left(\frac{\omega_{n,a}^2}{\omega_{n,w}^2} - 1 \right) = \left(\frac{338.68^2}{116.70^2} - 1 \right) = 7.42 \tag{34}$$

where the natural frequency ω_n^* without the added-mass effect (as in Eq. (28))

$$\omega_n^* = \beta_1^2 \sqrt{\frac{EI}{\rho_b A_b}} \tag{35}$$

which is the same in water as in air, is approximated by the natural frequency in air $\omega_{n,a}$ because the added-mass effect is expected to

be relatively negligible in air due to the low density of air when compared with water, i.e.,

$$\omega_n^* \approx \omega_{n,a} \tag{36}$$

The effective hydrodynamic area A_w that contributes to the added-mass effect as the beam oscillates in water can be quantified in terms of the height H of the beam as (using Eq. (13))

$$A_w = \gamma H^2 = C_m\left(\frac{\rho_b A_b}{\rho_w}\right) \tag{37}$$

The density of the PDMS cilia (which ranges from 940–1000 $\mathrm{kg/m^3}$ is similar to the density 1000 $\mathrm{kg/m^3}$ of DI water. Therefore, the coefficient γ (in Eq. (37)) can be estimated from the value of C_m in Eq. (34) and the cilia depth $D=10$ μm and height $H=45$ μm,

$$\gamma = C_m\left(\frac{\rho_b D}{\rho_w H}\right) = 7.42(10/45)\left(\frac{\rho_b}{\rho_w}\right) = 1.65\left(\frac{\rho_b}{\rho_w}\right) \tag{38}$$

to lie in the range

$$1.55 \leq \gamma \leq 1.65 \tag{39}$$

4.1.1 Comparison With Added-Mass Effect on Cylinder. Note that for a cylinder with cross section diameter H, the area A_{cyl} associated with added-mass term is [17] (Chap. 4),

$$A_{\mathrm{cyl}} = (\pi/4)H^2 = 0.785H^2 = \gamma_{\mathrm{cyl}}H^2$$

with $\gamma_{\mathrm{cyl}}=0.785$. Thus, the effective area (γH^2) influencing the added mass is about two times larger for cilia (γ in Eq. (39)) when compared with a cylinder with $2\gamma_{\mathrm{cyl}}=1.57$. This increase in the effective area for the cilia is anticipated since a thin rectangle of height H (with sharp edges) is expected to influence a larger fluid area when compared with a relatively smoother cylinder of cross-sectional diameter H.

4.1.2 Beam Density and the Added-Mass Effect. The added-mass effect captured by the added-mass coefficient $C_m=7.42$ (in Eq. (34)) depends on the relative density of the fluid and the beam material as in Eq. (13). In the current experimental setup, the density of the PDMS cilia is close to the density of the liquid (water). In contrast if the density of the beam is substantially larger (e.g., for metal or silicon-nitride cilia), then the added-mass effect would be much smaller. Thus, the significant added-mass effect in reducing the natural frequency of the cilia arises because, in addition to the geometry effect (i.e., the rectangular cross section), the density of the cilia is low.

4.2 Added Mass Reduces Resonance Frequency. It is shown that the added-mass effect substantially reduces the natural frequency (and thereby the resonant-vibrational frequency) in liquid. Moreover, it is shown that this substantial reduction in resonant-vibrational frequency cannot be due to the damping effect alone. The resonant-vibrational frequency is the frequency ω at which the magnitude of the transfer function in Eq. (2)

$$|G(j\omega)| = \left[\frac{(K-1)^2\omega^4 + 2(K-1)\omega^2\omega_n^2 + \omega_n^4 + 4(\zeta_2 - \zeta_1 K)^2\omega^2\omega_n^2}{\omega^4 + (4\zeta_2^2 - 2)\omega^2\omega_n^2 + \omega_n^4}\right]^{1/2}$$
$$= \left[\frac{(K-1)^2\left(\frac{\omega}{\omega_n}\right)^4 + 2[2\zeta_1^2K^2 + (1-4\zeta_1\zeta_2)K + 2\zeta_2^2 - 1]\left(\frac{\omega}{\omega_n}\right)^2 + 1}{\left(\frac{\omega}{\omega_n}\right)^4 + (4\zeta_2^2 - 2)\left(\frac{\omega}{\omega_n}\right)^2 + 1}\right]^{1/2} \tag{40}$$

is maximum. The magnitude is maximized when its square is maximized, or rather at the normalized frequency $\bar{\omega}$ that satisfies

$$\frac{d|G(\bar{\omega})|^2}{d\bar{\omega}} = 2|G(\bar{\omega})|\frac{d|G(\bar{\omega})|}{d\bar{\omega}} = \frac{d}{d\bar{\omega}}\left(\frac{P\bar{\omega}^2 + Q\bar{\omega} + 1}{\bar{\omega}^2 + R\bar{\omega} + 1}\right) = 0 \tag{41}$$

where

$$\bar{\omega} = \left(\frac{\omega}{\omega_n}\right)^2$$

$$P = (K-1)^2$$

$$Q = 2[2\zeta_1^2K^2 + (1-4\zeta_1\zeta_2)K + 2\zeta_2^2 - 1]$$

$$R = 4\zeta_2^2 - 2 \tag{42}$$

The optimization condition in Eq. (41) is equivalent to

$$(PR-Q)\bar{\omega}^2 + 2(P-1)\bar{\omega} + Q - R = 0 \tag{43}$$

and the resonant-vibrational frequency is given by

$$\bar{\omega}_r = \frac{\omega_r}{\omega_n} = \sqrt{\frac{(P-1) + \sqrt{(P-1)^2 - (Q-R)(PR-Q)}}{Q-PR}} \tag{44}$$

The normalized resonant-vibrational frequency $\bar{\omega}_r$ in Eq. (44) is shown in Fig. 3. Note from this figure that the maximum reduction in the resonant-vibrational frequency is about 10% of the natural frequency for damping ratios ζ_1 and ζ_2 less than 0.5 [5] because

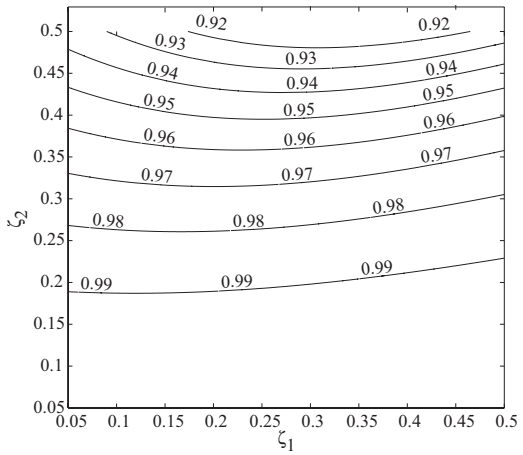

Fig. 3 Contour plot for normalized resonant-vibrational frequency $\bar{\omega}_r$ in Eq. (44)

Table 3 Columns 2–5: experimental fit of the parameters in Eq. (2) for cilia with different lengths L actuated in DI water with $K=1.566$. Columns 6–9: predicted natural frequencies $\omega_{n,w,p}$ and resonant-vibrational frequencies $\omega_{r,w,p}$ using parameters for the 800 μm cilia (in Table 2) and prediction errors $E_{n,w}, E_{r,w}$ as in Eq. (50). The predictions are not applicable (N/A) for the 800 μm case.

L (μm)	ζ_1	ζ_2	$\omega_{n,w}$ (Hz)	$\omega_{r,w}$ (Hz)	$\omega_{n,w,p}$ (Hz)	$E_{n,w}$ (%)	$\omega_{r,w,p}$ (Hz)	$E_{r,w}$ (%)
480	0.452	0.470	335.6	312.75	324.14	3.5	304.23	2.7
540	0.448	0.462	264.2	246.98	256.11	3.2	240.38	2.7
670	0.441	0.458	178.4	166.94	166.37	7.2	156.15	6.5
760	0.441	0.453	136.8	128.28	129.30	5.8	121.36	5.4
800	0.438	0.450	116.70	109.54	N/A	N/A	N/A	N/A

$$\bar{\omega}_r = \frac{\omega_r}{\omega_n} > 0.9 \tag{45}$$

Without the added-mass effect, the natural frequency in water $\omega^*_{n,w}$ would be the same as the natural frequency in air $\omega^*_{n,a}$, which in turn would equal ω^*_n in Eq. (35),

$$\omega^*_{n,w} = \omega^*_{n,a} = \omega^*_n \tag{46}$$

Therefore, the reduction in the resonant-vibrational frequency $\omega^*_{r,w}$ in water due to damping effect alone (without the added-mass effect) would not be significant; it would be less than 10% from Eq. (45), which predicts the resonant-vibrational frequency (without added mass) to be

$$\omega^*_{r,w} > 0.9\omega^*_{n,w} = 0.9\omega^*_n \approx 0.9\omega_{n,a} = 0.9(338.68) = 304.81 \text{ Hz} \tag{47}$$

from the approximation in Eq. (46). However, the observed natural frequency in water ($\omega_{n,w}=116.7$ Hz in Table 2) is substantially lower than the observed natural frequency in air ($\omega_{n,a}=338.68$ Hz in Table 1). This substantial reduction cannot be predicted by damping effects alone, without the added-mass effect. In contrast, the added-mass effect predicts a substantially lower natural frequency in water $\omega_{n,w}$ in comparison to the natural frequency in air $\omega_{n,a}$ by a factor of κ:

$$\kappa = \frac{1}{\sqrt{(1+C_m)}} = 0.345 \tag{48}$$

as in Eq. (28) with C_m from Eq. (34). The further relatively minor reduction in the resonant-vibrational frequency in water ($\omega_{r,w}=109.54$ Hz in Table 2) in comparison to the natural frequency in water ($\omega_{n,w}=116.7$ Hz in Table 2) is the result of the damping effect as in Eq. (44). Therefore, the added mass (and not the damping) has the dominant influence on the reduction in the natural frequency $\omega_{n,w}$ and, therefore, on the reduction in the resonant-vibrational frequency $\omega_{r,w}$ in liquid when compared with the natural frequency $\omega_{n,a}$ in air.

4.3 Added-Mass Effect on Cilia With Different Lengths. To evaluate the model of the added-mass effect, predictions of the resonant-vibrational frequency are comparatively evaluated against experimental results for cilia with different lengths. Cilia of different lengths were obtained by cutting the available, microfabricated 800 μm cilia. Since the cilia depth D and height H are the same, the cut cilia have the same cross-sectional area and, therefore, the added-mass coefficient C_m (in Eq. (13)) is expected to remain the same. Therefore, from Eqs. (24) and (28), the predicted natural frequency in water $\omega_{n,w}(L)$ for length L μm is related to the natural frequency in water (116.7 Hz in Table 2) for length 800 μm by

$$\omega_{n,w,p}(L) = 116.7\left[\frac{800}{L}\right]^2 \text{ Hz} \tag{49}$$

Moreover, the predicted resonant-vibrational frequency in water $\omega_{r,w,p}(L)$ for length L μm is obtained using the damping ratios for the 800 μm cilia (in Table 2) in Eq. (44) along with the predicted natural frequency $\omega_{n,w,p}(L)$ from Eq. (49). The parameters of the experimentally obtained model (in Eq. (2)), found by minimizing the least-squares-error between the predicted model response and measured frequency responses, are presented in Table 3. Moreover, the predictions (based on the 800 μm cilia) and the experimental values of the natural and resonant-vibrational frequencies are compared in Table 3, which shows that the model parameters from the 800 μm cilia can be used to predict the natural frequency and resonant-vibrational frequencies of the cut cilia to within 7.5% error, where the error is defined as

$$E_{n,w} = \frac{(\omega_{n,w} - \omega_{n,w,p})}{\omega_{n,w}} \times 100, \quad E_{r,w} = \frac{(\omega_{r,w} - \omega_{r,w,p})}{\omega_{r,w}} \times 100 \tag{50}$$

where the subscript p represents predicted values.

The fluid damping ratio $\zeta_f = \zeta_1$ (see Eq. (33)) is proportional to the square of the length L since it is inversely proportional to β_1^2 (see Eq. (29)), where β_1 is inversely proportional to the length L (Eq. (24)). However, the fluid damping ratio ζ_f is also proportional to the damping parameter B_f (in Eq. (29)), which depends on the flow conditions such as flow velocities—flow velocities tend to be lower at the lower vibrational frequencies investigated with longer cilia. Hence the fluid damping ratio $\zeta_1 = \zeta_f$ is not expected to vary proportionally with the square of the cilia length L in Table 3.

4.4 Added Mass Increases the Resonance Amplitude. In addition to the reduction in the natural (and resonant-vibrational) frequencies with the added-mass effect (as in Eq. (28)), from Eqs. (29) and (30), the fluid and internal damping ratios, ζ_f and ζ_i, are also reduced by the same factor $\kappa=0.345$ in Eq. (48). Therefore, the damping ratios ζ_f and ζ_i without the added-mass effect (denoted by the superscript "$*$") tend to be about three times ($1/\kappa = 2.898$ times) larger when compared with the case with the added-mass effect. In particular, for the 800 μm cilia, the damping ratios ζ_f and ζ_i without the added-mass effect are estimated to be (from Eqs. (29), (30), and (33))

$$\zeta^*_1 = \zeta^*_f = \frac{\zeta_f}{\kappa} = \frac{\zeta_1}{\kappa} = \frac{0.438}{0.345} = 1.27 \tag{51}$$

$$\zeta^*_2 = \zeta^*_i + \zeta^*_f = \frac{(\zeta_i + \zeta_f)}{\kappa} = \frac{\zeta_2}{\kappa} = \frac{0.45}{0.345} = 1.3 \tag{52}$$

The added-mass effect effectively decreases the damping ratio (when compared with the model without the added mass) and

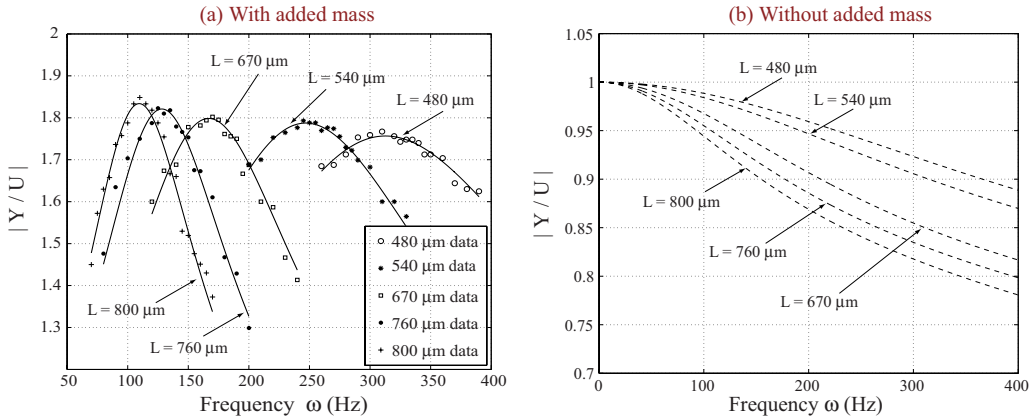

Fig. 4 Frequency response prediction in water for models of cilia (with different lengths): (*a*) with the added-mass effect (solid lines) and (*b*) without the added-mass effect (dashed lines). Experimentally measured data points are shown in the left plot.

thereby increases the vibrational response at the resonance. In particular, without the added-mass effect, the system is overdamped with damping ratio greater than 1 (i.e., $\zeta_2^*=1.3$); the maximum expected amplitude of vibration is then 1 (i.e., the same as the applied base motion). In contrast, with the added-mass effect, the system is underdamped with damping ratio less than 1 (i.e., $\zeta_2=0.45$); the ensuing maximum amplitude at resonance is expected to be greater than 1. This increase in the amplitude at the resonance frequency with the added-mass effect is seen in Fig. 4, which compares the models with and without the added-mass effect for different cilia lengths. Note that the model with the added-mass effect captures the experimental data well as opposed to the model without the added mass (that predicts an overdamped system). Thus, the added-mass effect is needed in the model to capture both (i) the substantial reduction in the resonant-vibrational frequency of the cilia in liquid when compared with air and (ii) the relatively large amplitude at resonance even in the presence of substantial fluid damping due to an effective reduction in the damping ratio.

5 Conclusions

This article showed that the added mass due to fluid-structure interaction significantly affects the vibrational dynamics of cilia-based (vibrating cantilever-type) devices proposed for handling the micro-/nanoscale fluid flows. Furthermore, it showed that the damping effects of the hydrodynamic interaction between the cilia-based actuators and fluid cannot fully explain the substantial reduction (by about a third) in the resonant frequency of the cilia actuators in liquid when compared with the natural frequency in air. The article showed that an added-mass effect explains (i) this reduction in the resonant frequency due to an increase in the effective inertia and (ii) the relatively large amplitude at resonance, even in the presence of substantial fluid damping, due to an effective reduction in the damping ratio.

Acknowledgment

This work was funded by the National Science Foundation Grant No. CMII 0624597. S.D. is grateful for the support from the National Science Council of Taiwan Grant No. NSC 96-2221-E-006-245, for a sabbatical visit to the National Cheng Kung University, Tainan, Taiwan.

References

[1] Oh, K., Chung, J.-H., Devasia, S., and Riley, J. J., 2009, "Bio-mimetic Silicone Cilia for Microfluidic Manipulation," Lab Chip, **9**(11), pp. 1561–1566.
[2] Yum, K., Wang, Z., Suryavanshi, A. P., and Yu, M.-F., 2004, "Experimental Measurement and Model Analysis of Damping Effect in Nanoscale Mechanical Beam Resonators in Air," J. Appl. Phys., **96**(7), pp. 3933–3938.
[3] Zhang, C., Xu, G., and Jiang, Q., 2003, "Analysis of the Air-Damping Effect on a Micromachined Beam Resonator," Math. Mech. Solids, **8**, pp. 315–325.
[4] Zhang, W., and Turner, K., 2007, "Frequency Dependent Fluid Damping of Micro/Nano Flexural Resonators: Experiment, Model and Analysis," Sens. Actuators, A, **134**(2), pp. 594–599.
[5] Chon, J. W. M., Mulvaney, P., and Sader, J. E., 2000, "Experimental Validation of Theoretical Models for the Frequency Response of Atomic Force Microscope Cantilever Beams Immersed in Fluids," J. Appl. Phys., **87**(8), pp. 3978–3988.
[6] Burns, D. W., Zook, J. D., Horning, J. D., Herb, W. R., and Guckel, H., 1995, "Sealed-Cavity Resonant Microbeam Pressure Sensor," Sens. Actuators, A, **48**, pp. 179–186.
[7] Burns, D. W., Horning, J. D., Herb, W. R., Zook, J. D., and Guckel, H., 1996, "Sealed-Cavity Resonant Microbeam Accelerometer," Sens. Actuators, A, **53**, pp. 249–255.
[8] Newell, W. E., 1968, "Miniturization of Tuning Forks," Science, **161**, pp. 1320–1326.
[9] Nise, N. S., 2004, *Control Systems Engineering*, 4th ed., Wiley, Hoboken, NJ.
[10] Hosseini, M. K. A., Omidi, O., Meghdari, A., and Vossoughi, G., 2006, "A Composite Rigid Body Algorithm for Modeling and Simulation of an Underwater Vehicle Equipped With Manipulator Arms," ASME J. Offshore Mech. Arct. Eng., **128**, pp. 119–132.
[11] Stokes, G. G., 1850, "On the Effect of the Internal Friction of Fluids on the Motion of Pendulums," Trans. Cambridge Philos. Soc., **9**(2), pp. 8–106.
[12] Dareing, D. W., Thundat, T., Jeon, S., and Nicholson, M., 2005, "Modal Analysis of Microcantilever Sensors With Environmental Damping," J. Appl. Phys., **97**, p. 084902.
[13] Inman, D. J., 2001, *Engineering Vibration*, 2nd ed., Prentice-Hall, Englewood Cliffs, NJ.
[14] Ferrers, N. M., ed., 1970, "Researches on the Vibration of Pendulums in Fluid Media," *Mathematical Papers of George Green*, Chelsea Publishing, New York.
[15] Lindholm, U. S., Kana, D. D., Chu, W.-H., and Abramson, H. N., 1965, "Elastic Vibration Characteristics of Cantilever Plates in Water," J. Ship Res., **9**, pp. 11–22.
[16] Landau, L. D., and Lifshitz, E. M., 1987, *Fluid Mechanics*, (Course of Theoretical Physics), 2nd ed., Pergamon, New York, Vol. 6.
[17] Sumer, B. M., and Fredsoe, J., 2006, *Hydrodynamics Around Cylindrical Structures*, (Advanced Series on Ocean Engineering), revised ed., World Scientific, Hackensack, NJ, Vol. 26.